Third-Order Nonlinear Optical Effects in Nanostructured Materials: A Comparative Review of Bio-Tellurium, Graphene, and Carbon Nanotube Hybrids

Seamus A. Curran[*1], Briana Y. Salinas[2], Fateema N. Zafar[2,3], Paula V. Perez[4], Christina A. Rodriguez[5]

[1]Department of Physics, University of Houston, 4300 University Dr, Houston, 77204, USA

[2]Department of Mathematics, University of Houston, 4300 University Dr, Houston, 77204, USA

[3]Department of Biology, University of Houston, 4300 University Dr, Houston, 77204, USA

[4]Department of Chemical Engineering, University of Houston, 4300 University Dr, Houston, 77204, USA

[5]Department of Electrical Engineering, University of Houston, 4300 University Dr, Houston, 77204, USA

*Corresponding Author

Abstract

This review presents an overview of the third-order nonlinear optical (NLO) behavior of biologically synthesized tellurium (Bio-Te) nanocrystals, graphene, and carbon nanotube (CNT) hybrids, emphasizing the role of dimensionality, chemical functionalization, and dispersion medium in tuning optical behavior. The motivation lies in advancing materials for photonic applications such as optical limiting (OL), where nonlinear phenomena like reverse saturable absorption (RSA), saturable absorption (SA), and nonlinear scattering are essential to meeting the growing demand for high-performance optical limiters and photonic devices. The review first explores the synthesis of Bio-Te nanocrystals produced via anaerobic bacterial reduction and dispersion with poly(m-phenylenevinylene-co-2,5-Dioctoxy-p-phenylenevinylene) (PmPV) to improve solubility and photonic interaction. The discussion turns to investigate graphene,

focusing on unoxidized graphene nanosheets synthesized via liquid-phase exfoliation (LPE) in γ-butyrolactone and stabilized using polymer nanocomposites such as PVK-functionalized reduced graphene oxide (RGO-PVK). Lastly, the review examines CNT-based nanohybrids composed of double-walled (DWNT), multi-walled (MWNT), and single-walled (SWNT) nanotubes, functionalized with fluorescein (FITC), rhodamine B (RITC), or fullerene C60, and dispersed in solvents such as DMF (dimethylformamide) and PmPV/Toluene. Characterization techniques such as UV-Vis, Raman spectroscopy, and open aperture Z-scan confirmed the presence of doping effects, π–π interactions, and enhanced NLO responses. These findings aim to guide future design of nonlinear optical materials for advanced applications in optical switching, photoprotection, and data modulation technologies.

Keywords

carbon nanotubes; graphene; nonlinear optics; optical limiting; tellurium

Introduction

Third-order nonlinear optical (NLO) phenomena support a multitude of critical photonic technologies such as optical switching, data modulation, signal processing, and optical limiting (OL). As the demand for high speed and low power optical devices continues to grow, the ability to tailor and enhance third-order responses becomes highly essential. Unlike second-order nonlinear effects, third-order nonlinearities are not limited to noncentrosymmetric materials, but are universally present, making them applicable to a wide range of materials. Traditional approaches to NLO materials have largely focused on chemically synthesized nanostructures, but recent innovations in green synthesis and hybrid composite engineering have opened new pathways for environmentally friendly and highly efficient alternatives. Among the most promising candidates are carbon-based nanomaterials such as carbon nanotubes (CNTs),

graphene and its derivatives, and more recently, biologically synthesized tellurium (Bio-Te) nanostructures.

Nonlinear optics describes the nonlinear effects resulting from high-intensity light propagating across a material, where the induced microscopic polarization (P) governs how the material interacts with light and is expressed as a function in terms of the electric field (E) given by

$$\boldsymbol{P} = \boldsymbol{\Sigma\alpha_{ij}E} + \boldsymbol{\Sigma\beta_{ijk}E^2} + \boldsymbol{\Sigma\gamma_{ijkl}E^3} + \cdots \qquad (1)$$

Here, $\boldsymbol{\alpha_{ij}}$ represents linear polarizability, $\boldsymbol{\beta_{ijk}}$ represents first hyperpolarizability, and $\boldsymbol{\gamma_{ijkl}}$ represents the second hyperpolarizability. This expansion of polarization in powers of the electric field classifies the nonlinear optical effects by order and reflects how a material interacts with light at increasing orders of field strength shown as a power series in E [1].

$$\boldsymbol{P} = \boldsymbol{\varepsilon_0}(\boldsymbol{\chi^{(1)}E} + \boldsymbol{\chi^{(2)}E^2} + \boldsymbol{\chi^{(3)}E^3} + \cdots) \qquad (2)$$

Each NLO susceptibility tensor $\boldsymbol{\chi^{(n)}}$ maps the interaction of n electric fields into a material response. In particular, third-order NLO behavior is described by $\boldsymbol{\chi^{(3)}}$, a fourth rank tensor governing third harmonic generation (THG), the optical Kerr effect, two photon absorption (TPA), and reverse saturable absorption (RSA) [2]. In centrosymmetric materials, where $\boldsymbol{\chi^{(2)}}$ = 0, third-order NLO effects dominate and become universally accessible across organic and inorganic systems. To characterize these processes, Z-scan techniques are widely employed. Open aperture Z-scan probes the imaginary part, Im[$\boldsymbol{\chi^{(3)}}$], capturing absorption related effects, while in contrast, closed aperture Z-scan probes the real part, Re[$\boldsymbol{\chi^{(3)}}$], corresponding to refractive nonlinearities such as self-focusing and refracting index changes [3]. Together, these measurements enable full characterization of a material's third-order nonlinear behavior, providing critical insight into both energy dissipation and refractive index changes under high

optical fields. Complementary techniques such as Raman spectroscopy, photoluminescence (PL) decay, and UV-Vis absorption spectroscopy provide further insight into the mechanisms in effect. Building on this founding, this study presents a comparative investigation into the synthesis, characterization, and nonlinear optical performance of three nanostructured systems: biologically synthesized tellurium (Bio-Te), solution-phase exfoliated graphene and graphene oxide (GO) polymer nanocomposites, and carbon nanotube (CNT) based hybrids functionalized with chromophores and fullerenes. The focus lies in understanding how dimensionality, synthesis strategy, chemical functionalization, and host matrix affect the optical behavior of such materials.

Tellurium, traditionally synthesized via chemical reduction methods, is reimagined through a green synthesis route involving Bacillus selenitireducens, which reduces tellurite (Te IV) ions into elemental Te(0). The result is the formation of 2D nanocrystalline rosettes through a natural biomineralization process [4]. To address the issue of dense aggregation that hinders optical interaction, the Bio-Te is dispersed in poly(m-phenylenevinylene-co-2,5-dioctoxy-p-phenylenevinylene) (PmPV) dissolved in toluene, enabling π–π interactions that promote uniform solubility and enhance photonic coupling [4]. Further integration into PMMA films has allowed nonlinear behavior to be studied in solid-state devices. Characterization via HRTEM, Raman spectroscopy, UV-Vis, PL decay, and Z-scan has revealed significant SA and nonlinear extinction (NLE) under femtosecond and nanosecond excitation, with a broadband response extending from the visible to mid-infrared [4]. Notably, the nonlinear performance of Bio-Te-PmPV exceeds that of chemically synthesized Te and benchmark materials such as black phosphorus, graphene, and fullerene composites.

Graphene, produced via solution-phase exfoliation (LPE), offers broadband optical absorption, ultrafast carrier dynamics, and powerful third-order NLO behavior. In this review, unoxidized 2D graphene nanosheets are complemented by reduced graphene oxide (RGO)

synthesized through the Hummers method and functionalized with polyvinyl carbazole (PVK) in tetrahydrofuran (THF) to form RGO-PVK nanocomposites [5]. These materials exhibit strong OL effects through a combination of RSA, multi-photon absorption (MPA), and thermally induced scattering. Z-scan analysis shows strong broadband response under 532 nm and 1064 nm laser excitation, and the response is enhanced by the dispersant's surface tension and the polymer matrix's compatibility [5].

The nonlinear optic behavior and properties (NLO) of one-dimensional carbon nanotube (CNT) based nanohybrids that were covalently or noncovalently functionalized with organic chromophores and fullerene dispersed in solvents was overviewed as well as their respective synthesis methods, materials, and NLO performance. The focus is on the hybrids composed of double-walled carbon nanotubes (DWNTs), multi-walled carbon nanotubes (MWNTs), and NanoBuds (SWNT based hybrid) that were functionalized with fluorescein isothiocyanate (FITC), rhodamine B isothiocyanate (RITC), and C60 fullerene that were then dispersed in DMF and/or PmPV/toluene. These hybrids exhibit exceptionally good NLO properties due to combined interactions between the carbon structure properties and the added moieties properties. The three major nonlinear mechanisms that were investigated as ways to evaluate their NLO behavior include reverse saturable absorption (RSA), photoinduced charge transfer, and exceptional thermally induced nonlinear scattering. Characterization was then performed using UV-Vis spectroscopy, Raman spectroscopy, and Z-scan technique to analyze the resulting effects. Systems like DWNT-C_{60}, MWNT-PVK, and MWNT-PCBF exhibit dual-mechanism optical limiting via both NLS and RSA [5]. Furthermore, CNT–polymer nanocomposites (e.g., MWNT-PVK, SWNT-PVK) synthesized through RAFT or in situ polymerization demonstrate excellent dispersion, long-term structural stability, and strong OL behavior at multiple wavelengths [5].

Together these three material systems, Bio-Te, graphene, and CNT-based hybrids, offer diverse nonlinear mechanisms and design strategies. This review provides a comprehensive analysis of their synthesis strategies, structural features, and NLO performance through a multitude of characterization techniques, highlighting key design principles such as the role of dimensionality, functionalization, and polymer compatibility. By comparing their third-order responses across multiple regimes and excitation conditions, we aim to identify material structure relationships that can inform the development of next-generation photonic protection technologies and integrated nonlinear optical devices.

Synthesis

Tellurium

The two-dimensional (2D) biological tellurium crystals were synthesized through a natural process which consisted of the anaerobic bacteria, Bacillus selenitireducens, placed in a lactate-Tellurite medium. The bacteria then processed Tellurite (Te IV) as respiratory electron acceptors and reduced it into elemental tellurium as the bacteria grew. Te(0) first appeared on the cell surface of the bacteria as nano-rods, then it accumulated into Te(0) shards, finally these shards exuviated as Te(0) rosettes. A procedure using Lysozyme and ultrasonication was employed to break the bacterial cells apart and achieve the separation and purification of Te(0) rosettes from the bacteria [6,7]. The Te(0) rosettes were washed and centrifuged numerous times. Finally, a conglomeration of Te(0) rosettes free of cellular debris was obtained.

The harvested Bio-Te nanostructures had dense aggregations that were unfavorable for both linear and nonlinear optical studies. Therefore poly(m-phenylenevinylene-co-2,5-dioctoxy-p-phenylenevinylene) (PmPV) was used to disperse the conglomeration of Te(0) forming a

nanocomposite of Bio-Te-PmPV. The fabrication of the Bio-Te-PmPV was achieved by adding the purified tellurium nanocrystals to a Toluene solution, then adding PmPV to this solution. The PmPV molecules have a coiled structure allowing them to enwrap the Bio-Te nanocrystals to the π-electron-richness of the PmPV. This enables close intermolecular proximity for π-π interactions to take place, obtaining effective dispersion of the Bio-Te aggregates. Bio-Te-PMMA films were created using a PMMA-Toluene solution to drop-cast into polymer petri dishes. The Toluene evaporated leaving behind the PMMA film. After the PMMA film dried, Bio-Te-PmPV solution was drop-cast on the surface of the PMMA film, the film was left to dry at room temperature for ten minutes, and the composite Bio-Te/PMMA film was successfully obtained.

Graphene

The technique used to synthesize 2D graphene was liquid-phase exfoliation (LPE). The y-butyrolactone was the solvent used to overcome the van der Waals force and successfully convert the graphene layer crystals into the unoxidized defect-free 2D graphene nanosheets [5, 8]. Graphene is insoluble in many organic solvents; to overcome this issue graphene oxide (GO) was created using the Hummers method. This GO was added to a N,N-dimethylformamide (DMF) solution to effectively disperse it.

To achieve solution-stabilized graphene polymer nanocomposites, the GO was thermally reduced and formed reduced graphene oxide (RGO) [9]. The RGO was then functionalized with Polyvinyl carbazole (PVK) by using sodium hydride (NaH) in tetrahydrofuran (THF) to generate anions in the main chain of PVK, followed by the nucleophilic addition of the anions into the RGO π-conjugated structure, forming the RGO-PVK nanocomposite.

Carbon Nanotubes Chromophores, Fullerenes and Nanotubes

Noncovalent composites, such as PmPV-CNT and PFO-CNT, are formed by dispersing CNTs in organic solvents (e.g., toluene, DMF) with conjugated polymers like PmPV. The polymers wrap around the nanotubes using π-π stacking, resulting in stable dispersions [5].

Covalent composites, however, follow more controlled synthesis routes. DWNT-C60 hybrids are prepared by grafting fullerene molecules onto amine-functionalized DWNTs using a polyethyleneimine (PEI) bridge. MWNT-PCBF is synthesized through a two-step process involving Suzuki coupling of the polymer followed by surface activation of MWNTs with acryl chloride for covalent attachment. MWNT-PVK is fabricated via RAFT polymerization using DDAT agents to help regulate PVK growth around MWNTs, while SWNT-PVK is formed through in situ anionic polymerization directly onto negatively charged SWNTs [3, 5].

These methods allow for precise control over coating thickness, solubility, and molecular architecture – elements that significantly impact OL performance [3,5]. Nonlinear optics (NLO) plays a major role in optical limiters, materials that allow low-intensity light to pass through but reduce high-intensity light. Carbon nanotubes (CNTs) are used as effective base platforms for many NLO materials due to their high thermal conductivity, one dimension (1D) pi-conjugated structure, broad absorption range, and high surface area. Unmodified or nonfunctionalized CNTs have poor dispersion in solvents and lack proper optical and electronic properties and therefore must be functionalized, or chemically modified, by attaching several moieties to further improve their NLO response [3, 5]. To fix these limitations, there is a process of covalently functionalizing CNTs with organic chromophores and noncovalently functionalizing CNTs with fullerene moieties that go on to create donor-acceptor systems that enhance charge transfer, nonlinear absorption, and scattering effects [3, 5].

The main structure materials included double-walled carbon nanotubes (DWNTs), multi-walled carbon nanotubes (MWNTs), and single-walled carbon nanotubes (SWNTs). The

DWNTs and MWNTs served as base platforms for the addition of chromophores, while SWNTs were used as the backbone for NanoBuds [5]. The chromophores FITC and RITC were used for functionalization as they showed strong visible absorption and contain functional isothiocyanate groups, which form covalent thiourea bonds with the rich amine-functionalized surfaces of PEI. The C60 fullerene was chosen for its significant RSA behavior [5]. The dispersion behavior was controlled using the polymer poly(m-phenylenevinylene-co-2,5-dioctoxy-p-phenylenevinylene) to facilitate and manage the π–π stacking with the CNTs. This leads to improved dispersion once combined with toluene due to its low boiling point and surface tension. Solvents also included dimethylformamide (DMF) for dissolving both PEI and helping disperse nanotubes [5].

To synthesize the PEI intermediate of the hybrids, DWNTs were dispersed in DMF and reacted with the n-dopant polyethylenimine (PEI) under sonication and stirred for five days. This introduced reactive nucleophilic amine electron donating groups on the nanotube surfaces. The product was isolated through filtration, washing, and drying procedures. The PEI-functionalized DWNTs were reacted with an excess of FITC or RITC in DMF for another five days, resulting in the formation of DWNT–FITC or DWNT–RITC hybrids through thiourea bond formation where their highly reactive isothiocyanate group form covalent bonds with the PEI amines. Similar synthesis procedures were conducted with MWNTs to form MWNT–FITC, MWNT–RITC, and MWNT–C60 hybrids. NanoBuds were noncovalently synthesized using an aerosol reactor system in which SWNTs were grown from carbon monoxide with ferrocene as a catalyst and CO_2 as an etching agent, promoting the growth of C60 fullerene structures directly on the outer CNT walls [5].

Characterization and Results

Tellurium

The crystal structure of the bacterially formed elemental tellurium nanoparticles was characterized by using High Resolution Transmission Electron Microscopy (HRTEM), Raman Spectroscopy, UV-Vis Absorption Spectroscopy, Photoluminescence (PL) Decay, Spectroscopic Ellipsometry, and open-aperture z-scan. These techniques allowed a deeper understanding of the NLO properties of Bio-Te and the potential photonic applications [4].

The dense aggregation of the purified Bio-Te is shown in Figure 1b obtained by HRTEM; the morphology of the Bio-Te rosettes suggested the low efficiency of the Bio-Te in linear and nonlinear optical studies [4]. Transmission Electron Microscopy was also used on the nanocomposite Bio-Te-PmPV (Figure 1d). The image obtained showed the trigonal crystal structure constituted of three Te atoms per unit cell, exhibiting covalent bonding that resulted in a concatenation of helical chains that interacted with each other by van der Waals forces.

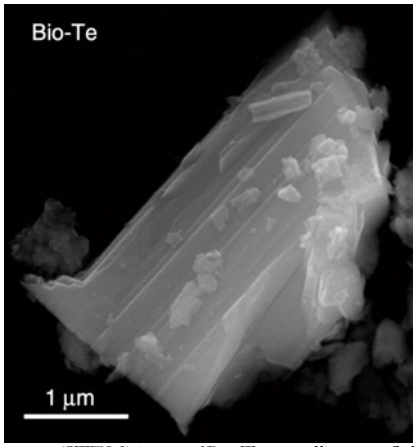

Figure 1b: *Scanning transmission electron microscopy (STEM) image of Bio-Te crystalline nanoflakes. Reproduced from [4], licensed under CC BY 4.0.*

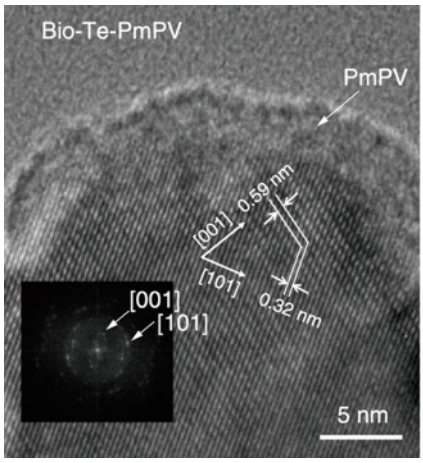

Figure 1d: *Transmission electron microscopy (TEM) image of a Bio-Te crystalline nanoflake wrapped by PmPV layers. Reproduced from [4], licensed under CC BY 4.0.*

Raman Spectroscopy was used to determine the atomic structure arrangement of pure Bio-Te and Bio-Te-PmPV. The spectra of both materials were compared to the spectra of chemically synthesized tellurium (Chem-Te), Chem-Te-PmPV, and pristine PmPV (Figure 1e). The results showed the characteristic bands present in the crystal structure of Te were also present in pure Bio-Te and Bio-Te-PmPV. There were additional peaks corresponding to tellurium Dioxide (TeO2) that are probably associated with the oxidation of Te(0) due to air exposure. The linear optical absorption spectrum of Bio-Te-PmPV was obtained by subtracting the pure PmPV spectrum. This showed a broad absorption at 1.9 eV (about 650 nm). This red shift occurred due to the shift from p-nonbonding valence band triplet to p-antibonding conduction band triplet [10].

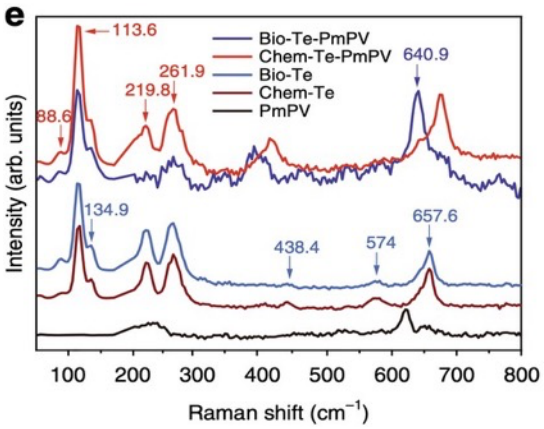

Figure 1e: *Raman spectra of Bio-Te, Bio-Te–PmPV, chemically synthesized tellurium nanocrystals (Chem-Te), Chem-Te–PmPV, and PmPV. Reproduced from [4], licensed under CC BY 4.0.*

Photoluminescence (PL) intensity spectra of Bio-Te-PmPV and PmPV were similar, exhibiting photoluminescence with broad peaks in the range between 450-650 nm. This suggests that the PmPV in the Bio-Te retained their PL, while the Te crystals showed no evidence of PL [4]. It is important to note that the PL of Bio-Te-PmPV was one order of magnitude lower than the PL of pure PmPV under the same conditions, which indicates that the Bio-Te nanocrystals suppressed the PL of the PmPV. The PL decay kinetics measurements showed that Bio-Te-PmPV decay is faster than pure PmPV for the first few ns. The two dominant tri-exponentials fit for the PL decay curve for Bio-Te-PmPV were about 338 ps and 1.09 ns, but for pure PmPV were 460 ps and 1.11 ns. One possible explanation for the quenching is the existence of energy transfer from the excited PmPV that acts as electron donor to the Bio-Te nanocrystals. The nonlinear (NL) properties of Bio-Te-PmPV were tested by multiple open-aperture z-scans with different wavelengths, excitations, and pulses [4]. To discover the nonlinear absorptive responses of Bio-Te-PmPV twelve different z-scans were taken. The first two were taken using 800 nm light with 100 fs pulses at $200\,\frac{nJ}{Pulse}$ and $400\ \frac{nJ}{Pulse}$. The results exhibit saturable absorption (SA) at $200\,\frac{nJ}{Pulse}$ but when the energy was increased to $400\,\frac{nJ}{Pulse}$ the results showed a dip at the center of the z-scan (z=0). This behavior suggests a combination of SA and nonlinear extinction

(NLE), the NLE effect being associated with the PmPV property of multiple-photon absorption (MPA). It is significant to note that PmPV did not exhibit any NLO properties by itself, therefore the NL effects are solely attributed to the Bio-Te nanocrystals. The photon transport equation was used to obtain the NLO coefficients for PmPV and Bio-Te. For laser excitations at 515 nm and 800 nm wavelengths, the PmPV presented two-photon absorption (TPA). The imaginary part of $\chi^{(3)}$ ($\mathrm{Im}\chi^{(3)}$) was calculated to tie the nonlinear susceptibility to the nonlinear absorption (α_{NL}) from the data obtained. This was then used to calculate the figure of merit (FOM) and the results showed that Bio-Te had a saturable absorption at least equivalent to that of Black Phosphorus (BP), which is a material known for its significant NL response.

Z-scan traces were also studied of Bio-Te-PmPV for 340 fs at 515 nm and 1030 nm laser pulses; this indicated the broad SA of the Bio-Te nanoparticles over the visible to near-infrared (NIR) wavelength range. The results showed that Bio-Te presents small amounts of SA in natural conditions, and for higher laser excitations (515 nm, 800 nm, and 1030 nm) it exhibits multiple-photon absorption (MPA). The saturation intensity (I_{sat}), FOM, and $\mathrm{Im}\chi^{(3)}$ of Bio-Te were obtained and compared to the known values for BP. At 1030 nm the I_{sat} for Bio-Te was about one-third that of BP, which implies a stronger SA response to Infrared (IR) light excitation [10].

To study the Bio-Te response to mid-infrared (MIR) light, the host for the Bio-Te nanocrystals was changed from PmPV to PMMA, due to the TPA and MPA properties of PmPV at MIR wavelengths [4]. The PMMA has a lower interference with light, which makes it a great host to isolate the Bio-Te nanocrystals NL effects. The composite Bio-Te-PMMA was subject to 35 fs laser pulses at 2.5μm and 2.8μm wavelengths. The results showed obvious SA at both wavelengths, which implies that the Bio-Te can work as a compliant mode-locker for ultra-fast mid-infrared fiber lasers. The SA responses were compared with those of graphene, which is notable NLO material for broadband SA over the visible to MIR spectrum.

Bio-Te was subject to 6 ns laser pulses at 1064 nm (IR) wavelength under three different intensities. The results showed NLE and SA behavior from the Bio-Te, at low laser intensity SA was the dominant NL effect, while the NLE completely dominated at high laser intensity. The results showed that the concentration of Bio-Te was directly proportional to the NLE effect. The optical limiting properties of Bio-Te-PmPV were compared to five other nonlinear extinction materials: PcZn (t-Bu_4PcZn), C_{60} fullerene, single-walled carbon nanotubes (SWCNTs), graphene, and graphene oxide (GO). The results demonstrated superior NLE effect by Bio-Te-PmPV over all the materials. This response is due to the light absorption efficiency, low heat capacity, and relatively low melting and boiling points. These properties give rise to micro-inhomogeneities that result in strong nonlinear scattering.

Ellipsometry was used to measure the refractive index of the Bio-Te-PMMA film as the temperature changed. The thermo-optic coefficient was calculated from the data obtained and compared to that of graphene and WS_2. The thermos-optic coefficient of Bio-Te-PMMA film was one to two orders of magnitude larger than those of graphene or WS_2, denoting that Bio-Te can induce a much larger phase change through thermos-optic effect.

The photonic applications of Bio-Te-PMMA were tested by inserting the film into a fiber laser system, first as a mode-locker, and then as Q-switcher. The performance of the Bio-Te nanocrystals in the laser system was satisfactory, showing similar outcomes as BP, graphene, and WS_2.

Graphene

The graphene and graphene composites were characterized using TEM, Raman spectroscopy, and z-scan methods. These techniques provided an insight into the nonlinear properties of graphene and the potential applications in optics nanotechnology [5].

The TEM and Raman spectrums were used to study the unoxidized single-layer graphene structure and morphology. The TEM results proved the existence of the monolayers and few-layer defect-free graphene, which indicates that the desired quality and structure was achieved. The Raman spectra showed a clear G, 2D band, and an absent D peak. These outcomes align with the previous morphology results from the TEM.

The z-scan was performed using a 6 ns pulse operated at 532 nm and 1064 nm wavelengths with a pulse repetition of 10Hz. The pulse energy was altered from 0.03mJ/pulse to 0.3mJ/pulse and the beam intensity varied from 0.2 GW/cm^2 to 2.0 GW/cm^2. A focus lens was set up at ~35° to the direction of the incident beam to monitor the scattered light from the material. The graphene exhibited broadband OL at the said wavelengths. NLS was responsible for the nonlinear behavior caused by the thermally induced solvent bubbles and micro plasmas. A model to estimate the radius of the bubbles was established as a function of the surface tension of the dispersant. The theoretical results demonstrated that a lower surface tension leads to larger bubbles, therefore increasing scattering. The graphene OL response was comparable to that of C_{60} and SWNTs, implying the potential use as host for optical limiters and other photonic applications. The optical limiting property of GO in DMF was studied using the z-scan technique. The results showed RSA effect under ns pulses and TPA effect under ps pulses at 532 nm wavelength. The hybrid material RGO-PVK was also studied and showed an effective combination of NLS and TPA responses at 532 nm and 1064 nm [9]. The pure PVK was subject to a z-scan study, and it showed no sign of nonlinear optical response, hence the NL response from the RGO-PVK is attributed solely to the RGO.

Carbon Nanotubes Chromophores, Fullerenes and Nanotubes

Ultraviolet-visible (UV-Vis) absorption spectroscopy was used to observe at which wavelengths a compound absorbs light and to detect red shifts in absorption bands resulting from dye

aggregation or charge transfer. It confirms the attachment of certain functional groups to the material as well as the type of chemical bonds or electronic structures that are present within [5]. A red-shift in the major absorption maxima relative (peak wavelength where the dye absorbs light) has moved to a longer wavelength (lower energy) to free dye spectra (when the dye is just by itself in the solution) indicated possible electronic coupling and aggregation on the CNT surface. When the dye is covalently or non-covalently linked to the surface of the CNT, the electrons can be slightly transferred or shared between them which changes the electronic structure of the dye. This causes it to absorb light at a lower energy (longer wavelength). Control experiments for aggregation performed (drop-cast films) showed no red-shift so the red-shift is likely due to the electron properties and behavior in the CNTs [5].

Raman spectroscopy was used to look into the molecular vibration of CNTs, focusing on the G-band (C-C bonds) at around 1580 cm^{-1}. There was a downshift/lowered frequency that showed C-C bonds had gotten weaker because of n-type doping due to charge transfer (FITC/RITC donate electrons to CNTs). The D-band also supports nanotube functionalization by detecting defects or disruptions such as when molecules are attached [3].

The open-aperture Z-scan technique is where nanosecond laser light is focused through the sample. The Z-scan shows a value of nonlinear extinction coefficients (Beff) when it comes to nonlinear absorption and scattering. Comparing values between dispersions in DMF and PmPV/toluene helps the understanding of the solvent's effects and properties on bubble formation and scattering efficiency [5]. UV-Vis analysis revealed significant red-shifts for DWNT–FITC (440 to 530 nm) and DWNT–RITC (550 to 580 nm), suggesting charge transfer interactions. Raman spectroscopy showed G-band downshifts indicating progressive n-doping and electron transfer. Z-scan analysis shows that MWNT hybrids exhibited the strongest optical limiting behavior as they had the highest nonlinear extinction coefficient (Beff). This was due to

the combined effects of RSA from the dye moieties and enhanced scattering from the nanotube structure. Samples dispersed (NanoBuds) in NMP, a solvent with high boiling point and surface tension which inhibits rapid bubble formation and diminishes scattering efficiency. But the samples dispersed in PmPV/toluene showed better performance due to better solvent properties that accelerate bubble formation (more scattering centers). Based on the characterization of the several nanohybrids, DWNTs and MWNTs are more stable and durable than SWNTs [5].

TEM imaging confirms uniform polymer coating across all systems, typically ranging from 10 to 25 nm in thickness. Noncovalent systems (e.g., PmPV-CNT) appear as well dispersed, deep green solutions, while covalent systems exhibit thicker encapsulation, higher weight content, and impressive long-term dispersion stability (up to one month at 5 g/L for MWNT-PCBF) [5].

Optical limiting tests conducted under nanosecond excitation at 532 nm (in some cases at 1064 nm) confirm that thermally induced NLS is the primary mechanism at play in most systems. Microbubble formation, thermal lensing, and refractive index modulation consistently indicate this effect [5]. Interestingly, DWNT-C60 also exhibits RSA, particularly at higher intensities, attributed to the fullerene component. Similarly, dye functionalized CNTs show charge-transfer induced red-shifts and Raman G-band downshifts, indicating electron donation to the CNTs [3,5].

Among all materials tested, MWNT-PVK and MWNT-PCBF stood out for their superior broadband and dual-wavelength OL response, while SWNT-PVK hybrids shine in achieving lower threshold and uniform dispersion. Collectively, these systems illustrate how molecular engineering of polymer-CNT interactions govern NLO behavior and photonic application viability [3, 5].

Conclusion

This review presented a comprehensive exploration of third-order nonlinear optics (NLO) of a diverse range of nanostructured materials emphasizing specific composites such as carbon nanotube (CNT)-based hybrid composites, innovative fullerene systems, graphene, and biologically synthesized tellurium nanostructures. These materials are specifically engineered to enhance third-order nonlinear optical responses for optical limiting applications [2, 4]. The materials were examined specifically for their potential in optical limiting (OL) applications, where nonlinear mechanisms such as nonlinear scattering (NLS), reverse saturable absorption (RSA), and multi-photon absorption (MPA) play crucial roles in suppressing high-intensity laser transmission.

Among the most effective OL materials reviewed were polymer-CNT nanocomposites. Noncovalent systems like PmPV-CNT and PFO-CNT demonstrated efficient OL behavior primarily through thermally induced NLS. These systems maintain the electronic integrity of CNTs while improving dispersion through π-π interactions with conjugated polymers, leading to stability and easily processable composites capable of broad-spectrum OL [5]. Covalently bonded systems, including DWNT-C60, MWNT-PCBF, MWNT-PVK, and SWNT-PVK all exhibited enhanced OL capabilities. The enhanced properties were due to stronger interfacial interactions and the contributions of multiple nonlinear mechanisms [3, 5]. For instance, DWNT-C60 hybrids combined spatial scattering from CNTs with the RSA from the fullerenes, achieving up to 80% attenuation of the incident laser intensity. The MWNT-PVK and the MWNT-PCBF systems stood out for their high structural stability, broadband OL performance, and dual-wavelength sensitivity. These benefits were enabled by controlled synthetics methods like RAFT and in situ polymerization, allowing for uniform coating, improved solubility, and optimized light-material interaction [3].

Additionally, the review also highlighted Biosynthesized tellurium nanocomposites, which exhibit NL and OL properties over a broad range of wavelengths, especially IR. The Biosynthesized tellurium nanocrystals exhibited great nonlinear optical behavior, particularly saturable absorption and nonlinear extinction, and proved to be even better than chemically synthesized nanomaterials at infrared wavelengths [4]. The satisfactory performance of this Biomaterial in fiber laser systems demonstrates the promising potential in a broad range of photonic applications [4].

Graphene and its nanocomposites were also studied. They demonstrated great potential as optical limiters, displaying great broadband NLO and OL effects [8, 11]. The excellent NL properties and lower cost production make graphene nanocomposites great contestants for the next generation photonic components, and in photonic and nano-electronic applications.

Drawing a comparative analysis across all the material systems revealed that dimensionality (0D fullerenes, 1D CNTs, 2D Te), electronic structure, functionalization method, and polymer compatibility are all crucial in determining OL efficiency [3, 5]. While thermally driven NLS remained the dominant mechanism, RSA and charge transfer effects significantly amplified the response under Raman analysis, and UV-Vis spectroscopy provided critical insights into these behaviors and the underlaying structural interactions [3, 5].

In summary, these findings reinforce the immense promise of engineered nanocomposites in photonic protection technologies. The hybrid systems reviewed not only offer tunable nonlinear responses across visible and near infrared wavelengths but also serve as design templates for future OL materials. As fabrication techniques improve and material understanding of these materials deepens, these multifunctional nanocomposites are expected to play an increasingly vital role in laser safety, optical switching and integrated photonic systems [12, 13].

Acknowledgments

The authors thank Bryan Hlavinka (Department of Biochemistry, University of Houston) for valuable discussions and technical guidance. We also acknowledge the support of Integricote, Inc. (https://www.integricote.com/) for providing material data.

References

[1] Fatima, Z.; Basha, H. A.; Khan, S. A. A review: An overview on third-order nonlinear optical and optical limiting properties of Schiff bases. *J. Mol. Struct.* **2023**, *1292*, 136062. https://doi.org/10.1016/j.molstruc.2023.136062.

[2] Rao, A. S. Overview on second and third-order optical nonlinear processes. arXiv **2018**, arXiv:1612.09399 [physics.optics]. https://doi.org/10.48550/arXiv.1612.09399.

[3] Wang, J.; Liao, K.-S.; Früchtl, D.; Tian, Y.; Gilchrist, A.; Alley, N. J.; Andreoli, E.; Aitchison, B.; Nasibulin, A. G.; Byrne, H. J.; Kauppinen, E. I.; Zhang, L.; Blau, W. J.; Curran, S. A. Nonlinear optical properties of carbon nanotube hybrids in polymer dispersions. *Mater. Chem. Phys.* **2012**, 133 (2–3), 992–997. https://doi.org/10.1016/j.matchemphys.2012.02.003.

[4] Wang, K.; Zhang, X.; Kislyakov, I. M.; Dong, N.; Zhang, S.; Wang, G.; Fan, J.; Zou, X.; Du, J.; Leng, Y.; Zhao, Q.; Wu, K.; Chen, J.; Baesman, S. M.; Liao, K.-S.; Maharjan, S.; Zhang, H.; Zhang, L.; Curran, S. A.; Oremland, R. S.; Blau, W. J.; Wang, J. Bacterially synthesized tellurium nanostructures for broadband ultrafast nonlinear optical applications. *Nat. Commun.* **2019**, *10*, 3985. https://doi.org/10.1038/s41467-019-11898-z.

[5] Wang, J.; Chen, Y.; Li, R.; Dong, H.; Ju, Y.; He, J.; Fan, J.; Wang, K.; Liao, K.-S.; Zhang, L.; Curran, S. A.; Blau, W. J. Graphene and carbon nanotube polymer composites for laser protection. *J. Inorg. Organomet. Polym.* **2011**, *21*, 736–746. https://doi.org/10.1007/s10904-011-9581-8.

[6] Switzer Blum J, Burns Bindi A, Buzzelli J, Stolz JF, Oremland RS. Bacillus arsenicoselenatis sp. nov., and Bacillus selenitireducens sp. nov.: two haloalkaliphiles from Mono Lake, California that respire oxyanions of selenium and arsenic. *Arch. Microbiol.* **1998**, *171*, 19–30. doi:10.1007/s002030050673.

[7] Baesman SM, Bullen TD, Dewald J, Zhang D, Curran S, Islam FS, Beveridge TJ, Oremland RS. Formation of tellurium nanocrystals during anaerobic growth of bacteria that use Te oxyanions as respiratory electron acceptors. *Appl. Environ. Microbiol.* **2007**, *73*, 2135–2143. doi:10.1128/AEM.02558-06.

[8] Wang, J.; Hernandez, Y.; Lotya, M.; Coleman, J. N.; Blau, W. J. Broadband nonlinear optical response of graphene dispersions. *Adv. Mater.* **2009**, *21*, 2430–2435. https://doi.org/10.1002/adma.200803616.

[9] Li P-P, Chen Y, Zhu J, Feng M, Zhuang X, Lin Y, Zhan H. Charm-bracelet-type poly(N-vinylcarbazole) functionalized with reduced graphene oxide for broadband optical limiting. *Chem. Eur. J.* **2011**, *17*, 780–785. doi:10.1002/chem.201002431.

[10] Hirayama M, Okugawa R, Ishibashi S, Murakami S, Miyake T. Weyl node and spin texture in trigonal tellurium and selenium. *Phys. Rev. Lett.* **2015**, *114*, 206401. doi:10.1103/PhysRevLett.114.206401.

[11] Feng, M.; Zhan, H.; Chen, Y. Nonlinear optical and optical limiting properties of graphene families. *Appl. Phys. Lett.* **2010**, 96, 033107. https://doi.org/10.1063/1.3279148.

[12] Silva, R. R.; Mejia, H. A. G.; Ribeiro, S. J. L.; Shrestha, L. K.; Ariga, K.; Oliveira, O. N., Jr.; Camargo, V. R.; Maia, L. J. Q.; Araújo, C. B. Facile synthesis of tellurium nanowires and study of their third-order nonlinear optical properties. *J. Braz. Chem. Soc.* **2017**, *28*, 58–67. https://doi.org/10.5935/0103-5053.20160145.

[13] Xu, Y.; Liu, Z.; Zhang, X.; Wang, Y.; Tian, J.; Huang, Y.; Ma, Y.; Zhang, X.; Chen, Y. A graphene hybrid material covalently functionalized with porphyrin: Synthesis and optical limiting property. *Adv. Mater.* **2009**, *21* (12), 1275–1279. https://doi.org/10.1002/adma.200801617.

Data Availability Statement

Data generated and analyzed is available from the corresponding author upon reasonable request.